ON MODELLING AND SIMULATION OF BUOYANCY-DRIVEN BALLOONS WITH EVOLVING ENVELOPES

Uldis Strautins, Maksims Marinaki, Vanesa Vevere
Institute of Mathematics and Computer Science, University of Latvia, Latvia
uldis.strautins@lu.lv, maksims.marinaki@lu.lv, vanesavevere@inbox.lv

Abstract. Accurate prediction of various flying object trajectories and landing zones is of importance in nowadays applications. The paradigm of coupled particle-fluid flows where the internal particle properties such as geometry, density etc. are coupled to the macroscopic characterization of the fluid such as pressure, temperature etc. appears in multitude of important applications, ranging from predicting the trajectories of weather and spy balloons to dynamics of bubbles or nanoparticles in chemical industry. Balloon trajectories' prediction requires coupling atmospheric advection with the evolution of balloon volume, buoyancy and gas content. In this work we extend a Lagrangian particle framework to helium-filled balloons with evolving elastic envelopes. The horizontal motion is prescribed by a three-dimensional wind field, while the vertical motion includes gravity, buoyancy, added mass and quadratic drag. The balloon radius is computed from the ideal gas law with a linearized elastic-membrane correction, and gas leakage and burst are included. The model is tested using two wind-field classes: radiosonde-derived fields over Latvia, with and without a pressure-corrected vertical wind, and a synthetic mountain-ridge scenario representing controlled payload delivery. The simulations show two robust outcome families: balloons that lose gas and land whole and balloons that ascend, burst and descend by parachute. Landing positions are sensitive to payload mass, initial gas fill, vertical wind and wind shear, demonstrating the importance of coupling internal balloon dynamics with atmospheric transport.

Keywords: particulate flows, fluid dynamics, buoyancy, Lagrangian particles.

Introduction

The motion of buoyant objects through the atmosphere is governed by the interplay of gravitational, buoyancy, and aerodynamic forces, all of which depend on the ambient thermodynamic state. A helium-filled latex balloon is a prototypical example: as the balloon ascends, the decreasing ambient pressure causes its envelope to expand according to the ideal gas law, which in turn changes both the buoyant lift and the aerodynamic drag [1]. When the stretched envelope reaches a material-dependent critical radius the balloon bursts; otherwise, gas leaking through the latex membrane gradually reduces buoyancy and the balloon descends [2].

Accurate trajectory prediction for such objects has attracted renewed attention. In atmospheric science, radiosonde balloons are launched routinely, and their landing zones must be forecast for instrument recovery [3]. In the security domain, the 2023 surveillance-balloon incidents demonstrated that predicting the path of an uncooperative airborne object in real time is operationally critical [4]. Lagrangian trajectory models, notably the NOAA HYSPLIT system [5], have been the workhorse tool for air-parcel tracking, but they treat the transported object as a massless tracer and therefore cannot account for the coupled internal dynamics - radius evolution, gas leakage, burst - that determine whether, where, and how fast a balloon descends.

A rigorous treatment of a finite-size particle in a nonuniform flow leads to the Maxey-Riley equation [6], which includes buoyancy, added-mass, Stokes drag, and the Basset history force. For macroscopic balloons the Reynolds number is large, and the drag must be modelled empirically; Sobester et al. [3] proposed a stochastic sphere-drag model calibrated on thousands of radiosonde flights. Monte-Carlo ensembles built on such models yield probabilistic landing zones, but the coupled evolution of the balloon internal state - radius, membrane stress, gas content - is usually simplified to an algebraic burst criterion.

In the present work we extend our previously developed Lagrangian particle framework [7; 8] to the problem of buoyancy-driven balloons with fully coupled internal dynamics. The framework resolves: (i) horizontal advection by a three-dimensional wind field, (ii) vertical motion including inertia, buoyancy, and quadratic drag with an added-mass correction, (iii) balloon radius evolution from the ideal gas law with a neo-Hookean membrane correction, and (iv) helium loss through diffusion. Two categories of wind fields are tested: one derived from Latvian radiosonde data [9] and one entirely synthetic, corresponding to a smuggling scenario over mountainous terrain.

The two wind-field classes were selected to test complementary uses of the framework. Wind fields 1a and 1b provide a data-driven case based on locally available radiosonde observations and isolate the influence of including a reconstructed vertical wind component. Wind field 2 is an idealized operational scenario in which terrain, wind shear and delivery outcomes can be examined without dependence on a particular historical event.

Materials and methods

Atmospheric data and wind fields. Radiosonde observations from the Latvian Environment, Geology and Meteorology Centre (LVĢMC) open-data portal [9] form the basis of the first set of experiments. The data cover the south-eastern part of Latvia and include horizontal wind components u, v, pressure, and temperature at standard levels. Since full four-dimensional reanalysis data were not available for this study, the following processing was applied.

Wind field 1*a* (*calm*). A stationary wind field was constructed by ignoring the temporal variability of the soundings. Data were interpolated onto a regular grid using trilinear interpolants. Because the vertical wind component w was not present in the dataset, we set $w = 0$, corresponding to calm synoptic conditions.

Wind field 1*b* (*pressure-corrected*). To simulate vigorous convective conditions with up- and downdrafts, we computed w by projecting the field $(u, v, 0)$ onto stationary compressible fields satisfying $\nabla\cdot(\rho v) = 0$ through an iterative finite-volume pressure-correction algorithm. The air density ρ was obtained from interpolated pressure and temperature fields via the ideal gas law.

Wind field 2 (*synthetic scenario*). A fully synthetic scenario was designed as an idealized controlled payload-delivery problem: balloons carrying payloads are launched from one side of a mountain ridge and are collected on the other side. Air temperature and pressure depend only on altitude z and are estimated from the ISO 2533 Standard Atmosphere [10]. The wind field is prescribed analytically with altitude-dependent shear and incorporates terrain effects; the terrain itself is a smooth synthetic surface with peaks reaching approximately 3,000 m.

In this reduced model horizontal slip relative to the resolved wind is neglected, so $v_x - u = v_y - v = 0$. Consequently, the drag term below is applied only to the vertical relative velocity $v_z - w$. This approximation is appropriate when horizontal momentum relaxation is short compared with the time scale of changes in the resolved wind field; unresolved gusts, payload pendulum motion and horizontal inertial slip are therefore outside the present scope.

The balloon is assumed to move with the local wind velocity in horizontal directions: $\dot{x} = u\,(x, y, z)$, $\dot{y} = v\,(x, y, z)$; in the vertical direction we include inertia, buoyancy and drag:

$$\dot{z} = v_z;\; m_{eff}\dot{v}_z = (\rho V_b - m_{tot})g - \frac{1}{2}C_D\rho A|v_z - w|(v_z - w), \tag{1}$$

where $V_b = 4/3\ \pi\ r^3$ – balloon volume;
$A = \pi\ r^2$ – cross section area;
$C_D = 0.47$ – drag coefficient on a sphere;
$m_{tot} = m_{dry} + n_g\ M_{He}$ – total mass of balloon with payload;
$m_{eff} = m_{tot} + 1/2\ \rho\ V_b$ – effective mass with added-mass correction for an accelerating sphere [1].

The instantaneous balloon radius from ideal gas law for a linearized neo-Hookean balloon with unstretched thickness t_0, shear modulus G is

$$r(z, n_g) = \left(\frac{3n_g R_g T(z)}{4\pi P(z)}\right)^{\frac{1}{3}} - \frac{2Gt_0}{3P_0}, \tag{2}$$

The radius expression is used here as a first-order pressure-radius relation for an elastic spherical membrane; pressure-radius models for rubber balloons are discussed by Merritt and Weinhaus [15].

Gas loss due to leakage is estimated from Fick's law, using an Arrhenius-type temperature dependence of the rubber permeability [11]; a linearized approximation gives

$$\dot{n}_g = -\alpha \frac{T}{T_{ref}} \frac{r}{r_{ref}} n_g \,. \tag{3}$$

Balloons are supposed to burst when balloon radius reaches a specified burst radius r_{burst}. After a balloon bursts, it descends with the payload as a parachute. As a result, our model accounts for two modes of payload delivery: the balloon either reaches stratosphere and bursts or lands gently by gradually losing gas.

Results

Wind field 1: *radiosonde-based experiments*

Fig. 1 (left) shows 3-D trajectories for a mixed population of balloons with different payload masses launched from a single site under Wind field 1a (calm, $w = 0$).

Five initial helium amounts n_g (0) ∈ {75, 100, 125, 150, 175} [mol] were tested. Lighter payloads rise rapidly, their envelopes expanding until burst occurs in the upper troposphere, after which the payload descends under a parachute. Heavier payloads never generate sufficient buoyancy and descend whole after gradual gas leakage. The right panel of Fig. 1 shows the same experiment with all payloads set heavy: in this case no bursts occur and all balloons land within a comparatively compact zone.

When the pressure-corrected vertical wind (Wind field 1b) is activated (Fig. 2), the trajectories separate into two distinct families.

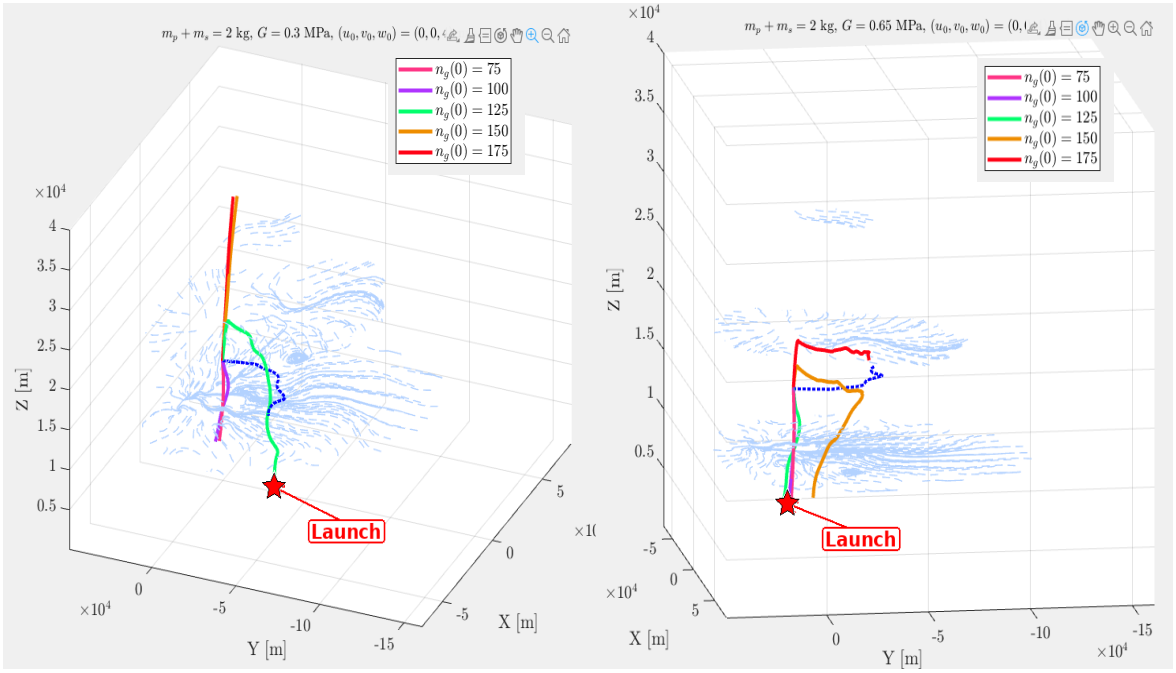

Fig. 1. **Wind field 1a ($w = 0$).** Colours denote n_g(0); red labels mark the launch points. Left: mixed light/heavy payloads. Right: all payloads are heavy, and no burst occurs

Colour denotes the initial helium amount n_g(0), while the payload class is identified by the resulting mode of motion: heavy-payload cases descend and land whole, whereas light-payload cases ascend to burst and then descend by parachute. The limiting case (blue dashed trajectory) corresponds to near-neutral buoyancy – a critical gas-fill level at which the balloon neither rises nor descends on the relevant time scale. Light-blue streamlines visualize the underlying wind field.

The right panel of Fig. 2 illustrates the effect of an elevated launch site under Wind field 1b. The wide dispersion of landing sites highlights the sensitivity of the outcome to the interplay between initial altitude, gas content, and the three-dimensional wind structure.

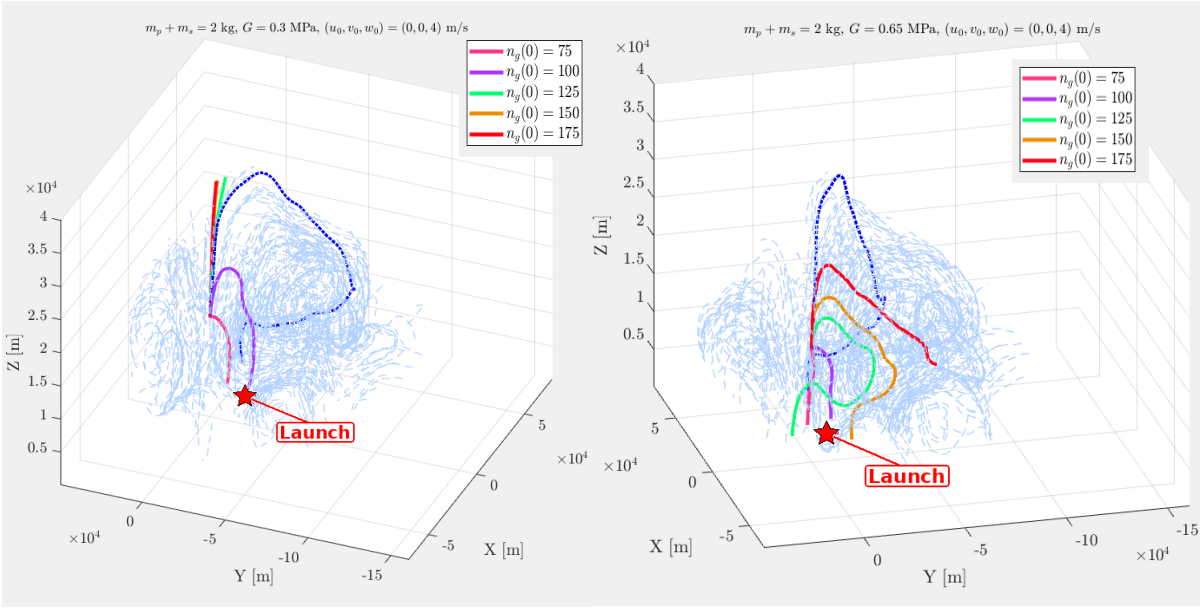

Fig. 2. **Wind field 1b with pressure-corrected vertical wind.** Colours denote $n_g(0)$; red labels mark the launch points. Left: whole-landing and burst-and-parachute families. Right: elevated launch site for the heavy-payload case. Light-blue lines are streamlines; the blue dashed path is the near-neutral-buoyancy case

Wind field 2: *synthetic scenario*

The synthetic mountain-ridge scenario is summarised in Fig. 3-5. Fig. 3 shows the prescribed wind field at four altitudes: a weak surface flow, a south-easterly jet near 3.5 km, and an upper-level flow at 9 km. A background hodograph reveals the wind veering with height. Fig. 4 shows all balloon trajectories over the terrain surface, with launch points, burst/crash events and delivery points indicated by the markers.

Fig. 5 (left) presents a plan-view map of ground tracks with landing-site markers identified by outcome (delivered, burst/crash, or short). The right panel shows the corresponding side-view (x-z plane): solid lines indicate the inflated-flight phase and dashed lines indicate the parachute-descent phase after burst. In both panels, red curves denote burst/crash cases and green curves denote delivered cases; ridge crests are indicated by shaded bands for reference.

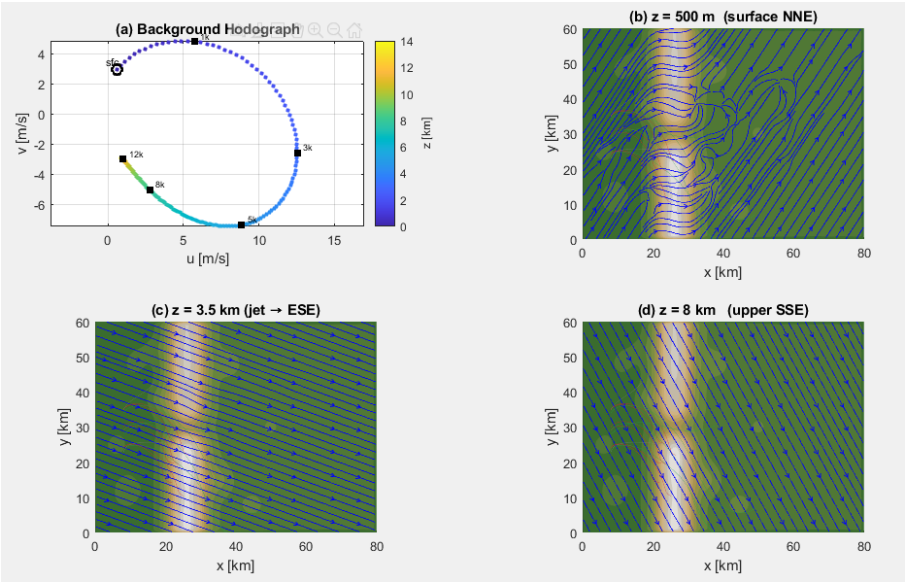

Fig. 3. **Wind field 2:** hodograph and selected-altitude wind fields over the synthetic ridge

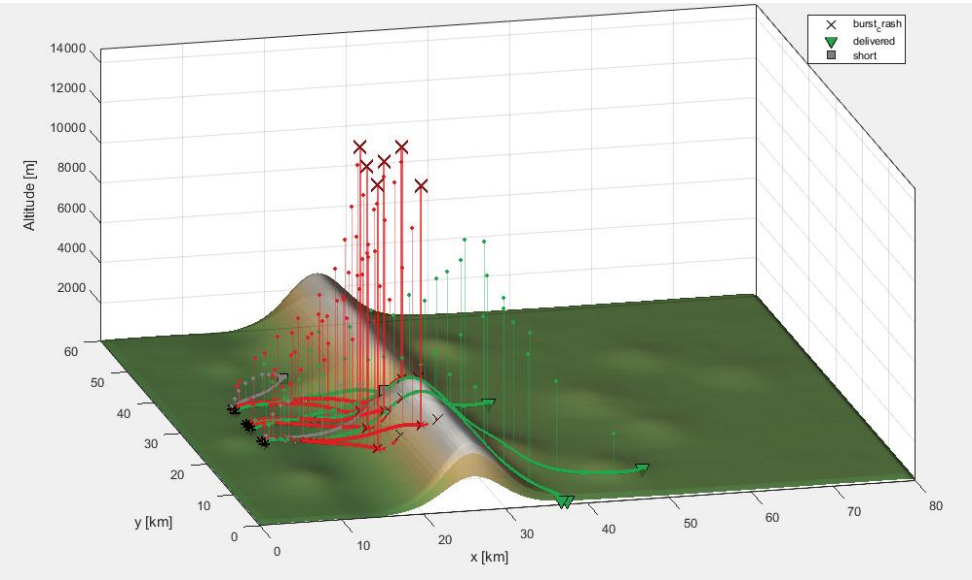

Fig. 4. **Wind field 2:** 3-D trajectories; red curves are burst/crash cases, green curves are delivered cases, and markers follow the legend

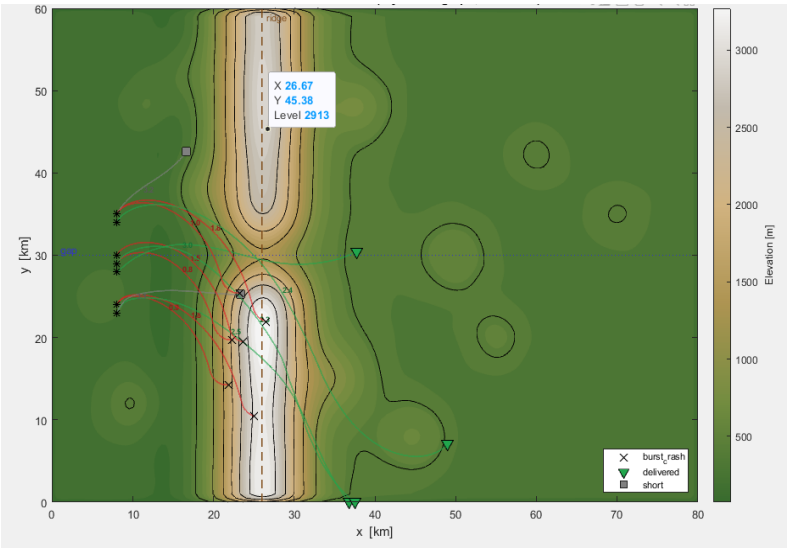

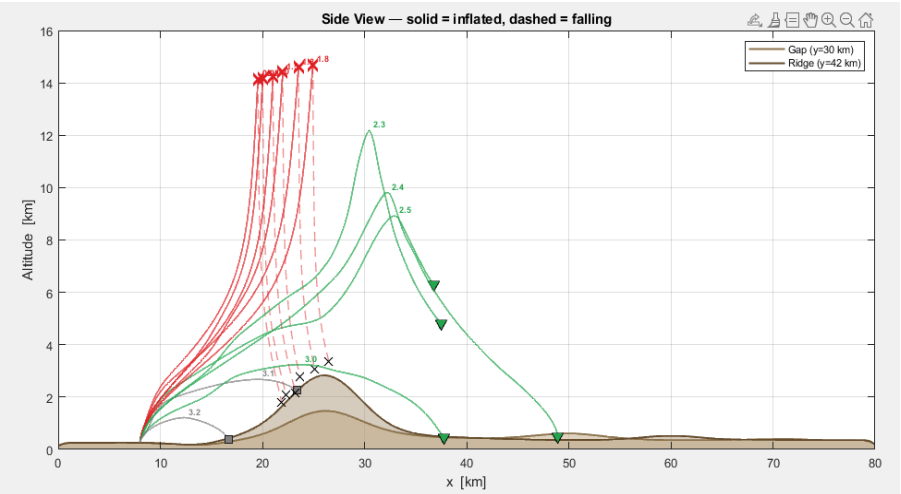

Fig. 5. **Wind field 2:** plan-view trajectories and landing markers over topography (top) and side view in the x-z plane; red curves indicate burst/crash cases and green curves indicate delivered cases; dashed segments show descent after burst (bottom)

Discussion

Several observations emerge from the experiments.

1. *Two delivery modes*. In all wind fields the balloon population naturally stratifies into "floaters'" that land gently after gas loss and "bursters" that reach high altitude before rapid descent. The payload mass and initial gas fill determine which mode is realised;
2. *Sensitivity to wind structure*. Wind shear between the surface and the jet-stream level rotates the horizontal ground track substantially. In the radiosonde-based experiments, introducing the pressure-corrected vertical wind ($w \neq 0$) causes landing sites to spread by several kilometres;
3. *Terrain interaction*. In the synthetic scenario, several heavy balloons impact the ridge. The terrain-following wind (not modelled here) would further complicate trajectories; coupling the particle solver to a mesoscale flow solver is a planned extension;
4. *Gas-leakage time scale*. For the leak-rate constant used ($\alpha \approx 10^{-4}$ s^{-1} at the reference conditions), a balloon losing gas without bursting can remain aloft for 30-60 minutes, which is sufficient to cross the 80km domain in the synthetic scenario.

Qualitative model assessment is now discussed. A flight-by-flight validation was not possible because GPS-tracked launches for the selected wind fields were not available. Nevertheless, the simulated behaviour is consistent with reported high-altitude balloon trajectory models: the predicted ascent, burst and parachute-descent family agrees qualitatively with the radiosonde balloon regime modelled by Sobester et al. [3], and the strong sensitivity of landing points to wind-profile and parameter uncertainty is consistent with the uncertainty studies of Palumbo et al. [13] and Lee and Yee [14]. The whole-landing family corresponds to the real situation in which leakage and payload mass reduce net buoyancy before the burst radius is reached. Quantitative validation against tracked local launches remains a necessary next step.

Conclusions

1. A Lagrangian particle framework coupling three-dimensional wind advection with internal balloon dynamics (radius evolution, membrane elasticity, gas leakage, burst) has been developed and implemented in Matlab.
2. Two categories of wind fields were tested: one derived from Latvian radiosonde observations and one fully synthetic. In both cases the model reproduces the physically expected bifurcation of trajectories into gently landing and bursting families.
3. Landing-site locations are highly sensitive to payload mass, initial gas fill, balloon material parameters, and the vertical wind component, confirming that accurate atmospheric data are essential for any operational trajectory forecast.
4. The modular architecture of the framework allows straightforward extension to other coupled particle--fluid problems, including bubble dynamics in industrial flows and real-time security-response trajectory prediction.

Author contributions

Conceptualization, U.S. and M.M.; methodology, U.S. and M.M.; software, U.S., M.M. and V.V.; validation, U.S. and M.M.; formal analysis, U.S. and M.M.; investigation, U.S. and M.M.; data curation, U.S., M.M. and V.V.; writing – original draft preparation, U.S. and M.M.; writing – review and editing, U.S. and M.M.; visualization, U.S., M.M and V.V. All authors have read and agreed to the published version of the manuscript.

References

[1] Batchelor G.K. An Introduction to Fluid Dynamics. Cambridge University Press, Cambridge, 2000. 615p.
[2] Sobester A. Stratospheric Flight: Aeronautics at the Limit. Springer, New York, 2011. 239p.
[3] Sobester A., Czerski H., Zapponi N., Castro I.P. High-altitude gas balloon trajectory prediction: a Monte Carlo model. AIAA Journal, vol. 52(4), 2014, pp. 832-842, DOI: 10.2514/1.J052900.
[4] Feldscher K. The Chinese balloon incident and its implications for airspace surveillance. Harvard Kennedy School Belfer Center, Policy Brief, 2023.

[5] Stein A.F., Draxler R.R., Rolph G.D., Stunder B.J.B., Cohen M.D., Ngan F. NOAA's HYSPLIT atmospheric transport and dispersion modeling system. Bulletin of the American Meteorological Society, vol. 96(12), 2015, pp. 2059-2077, DOI: 10.1175/BAMS-D-14-00110.1
[6] Maxey M.R., Riley J.J. Equation of motion for a small rigid sphere in a nonuniform flow. Physics of Fluids, vol. 26(4), 1983, pp. 883-889, DOI: 10.1063/1.864230
[7] Strautins U., Marinaki M. On simulation of soft matter and flow interactions in biomass processing applications. Engineering for Rural Development, vol. 23, 2024, pp. 933-938.
[8] Barmina I., Valdmanis R., Kalis H., Marinaki M. Experimental and numerical study of the development of swirling flow and flame dynamics and combustion characteristics at biomass thermo-chemical conversion. Engineering for Rural Development, vol. 16, 2017, pp. 68-74.
[9] Latvijas Vides, Geologijas un Meteorologijas centrs. Atmospheric radiosonde observation data. [online] [10.01.2025]. Available at: https://data.gov.lv/dati/eng/dataset/atmosferas-radiozondesanas-noverojumu-dati
[10] ISO 2533:1975. Standard Atmosphere. International Organization for Standardization, Geneva, 1975.
[11] Edwards J.D., Pickering S.F. Permeability of rubber to gases. Scientific Papers of the Bureau of Standards, vol. 16, 1920, pp. 327-362.
[12] Maxey M.R. Simulation methods for particulate flows and concentrated suspensions. Annual Review of Fluid Mechanics, vol. 49(1), 2017, pp. 171-193, DOI: 10.1146/annurev-fluid-122414-034408
[13] Palumbo R., Morani G., Corraro F. Effective approach to characterization of prediction errors for balloon ascent trajectories. Journal of Aircraft, vol. 47(4), 2010, pp. 1331-1337, DOI: 10.2514/1.47005
[14] Lee Y., Yee K. Numerical prediction of scientific balloon trajectories while considering various uncertainties. Journal of Aircraft, vol. 54(2), 2017, pp. 768-782, DOI: 10.2514/1.C033998
[15] Merritt D.R., Weinhaus F. The pressure curve for a rubber balloon. American Journal of Physics, vol. 46(10), 1978, pp. 976-977, DOI: 10.1119/1.11486